Reduced-Order Modelling of Turbulent Jets for Noise Control

Michael Schlegel, Bernd R. Noack, Pierre Comte, Dmitry Kolomenskiy, Kai Schneider, Marie Farge, Dirk M. Luchtenburg, Jon E. Scouten and Gilead Tadmor

Abstract A reduced-order modelling (ROM) strategy is pursued to achieve a mechanistic understanding of jet flow mechanisms targeting jet noise control. Coherent flow structures of the jet are identified by the proper orthogonal decomposition (POD) and wavelet analysis. These techniques are applied to an LES data ensemble with velocity snapshots of a three-dimensional, incompressible jet at a Reynolds number of $Re = 3600$. A low-dimensional Galerkin model of a three-dimensional jet is extracted and calibrated to the physical dynamics. To obtain the desired mechanistic understanding of jet noise generation, loudest flow structures are distilled by a goal-oriented extension of the POD approach we term 'most observable decomposition' (MOD). Thus, a reduction of the number of dynamically most important degrees of freedom by one order of magnitude is achieved. Capability of the presented ROM strategy for jet noise control is demonstrated by suppression of loud flow structures.

Michael Schlegel, Dirk M. Luchtenburg, Jon E. Scouten, Bernd R. Noack
Berlin Institute of Technology MB1, Straße des 17. Juni 135, 10623 Berlin, Germany, e-mail: michael.schlegel@tu-berlin.de

Pierre Comte
Laboratoire d'Études Aérodynamiques - CNRS UMR 6609 / Université de Poitiers, CEAT, 43, rue de l'aérodrome, 86036 Poitiers Cedex, France, e-mail: pierre.comte@lea.univ-poitiers.fr

Dmitry Kolomenskiy, Kai Schneider
Centre de Mathématiques et d'Informatique and Laboratoire de Mécanique, Modélisation & Procédés Propres -CNRS UMR 6181 / Université de Provence (Aix-Marseille I), 39, rue F. Joliot-Curie, 13453 Marseille - Cedex 13, France, e-mail: dkolom@lm3.univ-mrs.fr

Marie Farge
Laboratoire de Météorologie Dynamique - CNRS UMR 8539 / Ecole Normale Supérieure, 24, rue Lhomond, 75231 Paris - Cedex 05, e-mail: farge@lmd.ens.fr

Gilead Tadmor
Northeastern University, 440 Dana Building, 360 Huntington Avenue, Boston, MA 02115-5000, USA e-mail: tadmor@coe.neu.edu

1 Introduction

Jets from engine exhaust constitute the most important noise source of civil aircrafts during take-off. The noise level exceeds those of other sources like fan, combustion, and airframe noise. Hence, the suppression of jet noise has been actively pursued from the beginning of civil air traffic with jet engines, leading mainly to larger bypass ratios. As the engine diameter reaches its practical limit, further noise reductions will benefit from an intuitive understanding of the mechanisms responsible for noise generation in turbulent, subsonic jets. Yet, this understanding is still in its infancy after more than five decades of jet noise research (cmp. e.g. [51]). The complexity of this problem is ascribed to the high dimensionality and broadband spectrum of the flow state attractor.

Currently, an opportunity for model-based jet noise reduction is opening up by the rapidly evolving field of reduced-order modelling (ROM) (cmp. [63]). Performance of ROM for flow control purposes is demonstrated for control of vortex shedding behind circular and D-shaped cylinders [65, 66, 2, 31, 48, 72, 19, 67] and control of cavity oscillations [36]. Reduced-order models have also enabled successful feedback control in shear flow experiments, e.g. for bluff-body drag reduction and mixing enhancements [23, 52]. Requisites for empirical analyses and modelling are data bases provided by computational aeroacoustics. Here, direct numerical simulations (e.g. [18]) and large eddy simulations (e.g. [10, 3]) contribute to the understanding of experimental data (e.g. [24]). Similar efforts are undertaken by vortex-filament models [22, 69, 44, 70].

Targeting the distillation of the desired mechanistic understanding for jet noise reduction, we pursue a ROM strategy, including the tasks of structure identification, dynamical modelling and control design (cmp. figure 1). Therefore, a velocity snapshot ensemble of an incompressible jet at Reynolds number $Re = 3600$ is utilised, provided by a large eddy simulation (see [33, 7] and the references therein).

A main ROM challenge is represented by flow structure identification, tailored for the purposes of modelling and control. Constituting a class of flow representations, coherent flow structures are known to be a cause of the noise, as noted already in Lighthill's classical paper in 1952 [35]. Indeed, the frequency of the local noise source scales approximately inversely with the size of the coherent structures [43]. That size increases in the streamwise direction by vortex merging, leading to a decrease of the dominant frequency. This relationship has been experimentally corroborated and employed in surprisingly effective frequency slice models [56]. Commonly, coherent structures are extracted from POD, decomposing the flow velocity most efficiently for the resolution of total kinetic energy. In present jet POD studies (e.g. [73, 21, 17]), POD dimensions of O(100) of dynamically important degrees of freedom are revealed, which poses a serious challenge for model-based noise control. The POD method and POD analysis results for the incompressible jet are presented in section 3.

Further key enablers for structure identification are represented by wavelet techniques, which were used to study turbulence in already in the early nineties [11, 39]. Since then different directions for wavelets and turbulence have been explored, e.g.

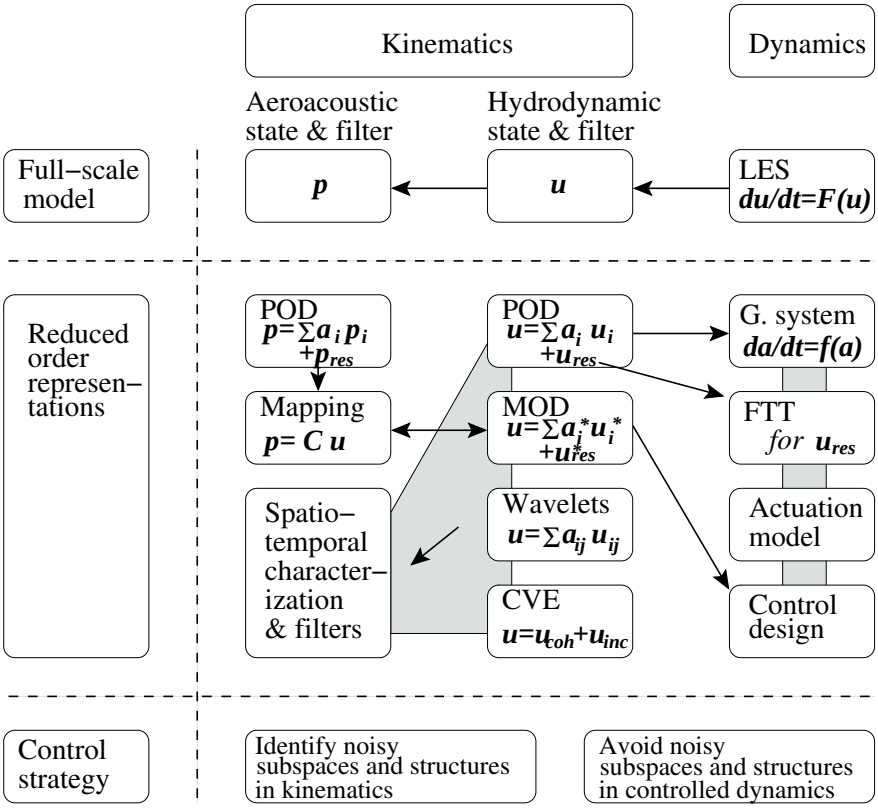

Fig. 1 Principle sketch of the reduced-order modelling (ROM) strategy, targeting jet noise control.

signal processing approaches, interpretations in the multifractal community, co-spectra, analysis and eduction of coherent structures using experimental data. In [15, 13] the Coherent Vortex Simulation (CVS) approach was introduced to compute and to model turbulent flows. The idea of CVS is to combine nonlinear approximation with denoising and, additionally, to exploit the properties of wavelets for numerical analysis. Wavelets yield attractive discretisations for operator equations. They allow auto–adaptive discretisations by estimating the local regularity of the solution. Furthermore, many integral and differential operators have a sparse representation in a wavelet basis and can furthermore efficiently be preconditioned using diagonal scaling. For a review we refer to the book of Cohen [6]. The idea of CVS is based on filtering turbulent flows using adaptive multiresolution techniques. Here the flow is split into two parts, a coherent flow, whose evolution is deterministically computed in an adaptive basis, and an incoherent flow, which is noise-like and whose effect on the coherent flow is modelled. Applications of this filtering, called Coherent Vortex Extraction, have been presented for homogenous isotropic

turbulence [14, 12, 50], for mixing layers [62] and for shear and rotating turbulence [28]. In this contribution methods and results of CVE are described in section 4.

To distill the desired mechanistic understanding for noise control, an acoustically optimised POD extension is applied for the identification of 'loud' coherent flow structures. In previous studies of compressible jets and mixing layers, typically a dimension reduction by one order of magnitude is achieved by this method, termed 'most observable decomposition' (MOD) (cmp. [61, 60, 29]). In these investigations, MOD modes exhibit the loudest flow structures which are interpreted in terms of known physical processes. In comparison to similar generalisations of the POD method (cmp. [16, 25, 4, 37, 17, 53], MOD is more tailored for the purposes of flow control: beside MOD's aeroacoustical least-dimensionality MOD features additional optimal properties as a design parameter. Thus, two MOD variants are proposed for controller and observer design. The reduction of the total kinetic energy in the subspace of the 'least-energetic' variant of MOD modes causes a reduction of the far-field fluctuation, thus enabling noise suppression by conventional energy-based control. The reconstruction of flow states from given aeroacoustic data, using e.g. dynamic observers, is supplied by the second variant of MOD modes, the 'least-residual' MOD modes. The MOD analysis and its results for the incompressible jet are contained in section 5.

Building on the kinematic results above, a further key enabler for flow and noise control is a portfolio of Galerkin modelling techniques addressing configuration-specific physical problems of dynamical systems. The challenges for model-based control of turbulent shear flows have been addressed by auxiliary models for the pressure term, unresolved turbulence, missing dynamically important phase space directions, compressibility effects and actuation effects [41, 34, 42, 71, 31, 46, 47, 75, 49]. Furthermore, turbulence effects are modelled by a turbulence closure generalising the ansatz of finite-time thermodynamics (FTT) [45]. This closure allows to predict the first and second moments of Galerkin modes, including the effects of fine-scale structures. For the prediction of first and second moments, effects of turbulent small-scale structures are modelled by a novel, model-based turbulence closure generalising the ansatz of finite-time thermodynamics (FTT) [45]. This FTT closure enables further system reductions and fine-scale turbulent representations respecting momentum and energy balance equations for each mode. FTT has already been successfully applied to wake flows, mixing layers and homogeneous shear turbulence, i.e. examples of simple, medium and broadband dynamics.

For the first time, a Galerkin model of the three-dimensional round jet is extracted in section 6 — utilising above mentioned ensemble of LES velocity snapshots. Thus, existing Galerkin models of rectangular and planar jets are supplemented (cmp. e.g. [40, 20] and references therein). In the outlook of this contribution (section 7), capability of the presented ROM strategy for jet noise control is demonstrated by first results from applications.

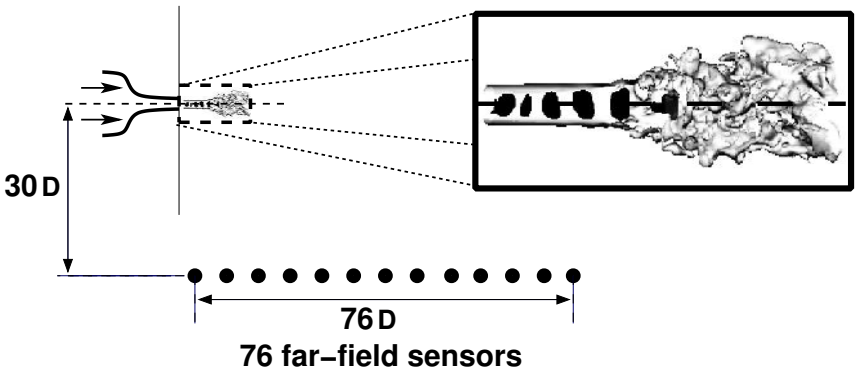

Fig. 2 Sketch of the flow configuration. A three-dimensional, incompressible jet is considered for the Reynolds number $Re = 3600$.

2 Configuration and data base

A snapshot ensemble of a three-dimensional incompressible jet at Reynolds number $Re = 3600$ is provided by large eddy simulation (LES). Details of the numerical simulations are illustrated in [33, 7]. For the subsequent empirical analyses, 3000 snapshots of velocity and pressure field in the post-transient regime are available in a domain extending $17D$ (D=jet diameter) in the streamwise x-direction and out to $\pm 3.5D$ in transverse y- and spanwise z-direction. In our computations, equations are discretised by a $128 \times 128 \times 128$ mesh of grid points, equidistantly distributed in each direction. The 3000 snapshots are equidistantly distributed over a time interval of 300 convective time units ($\Delta t = 0.1$). Furthermore, the three-dimensional vorticity field is provided for the last 1000 snapshots.

The aeroacoustic far-field is monitored by the signals of 76 far-field sensors, situated at a linear array in the zero plane of the spanwise component (cmp. figure 2). The linear array is parallel to the jet axis with a distance of $30D$. The sensors are equidistantly distributed from x=0D to x=75D. The aeroacoustic field is computed by a Green's function-based solver described e.g. in [27]. The solver is validated against the results of a Ffowcs-Williams Hawkings solver for a $Ma = 0.9$ jet configuration at the same Reynolds number (cmp. [21, 38]). Thus, aeroacoustic far-field data (cmp. figure 3) are provided in an interval of 100 convective time units based on the LES data described above.

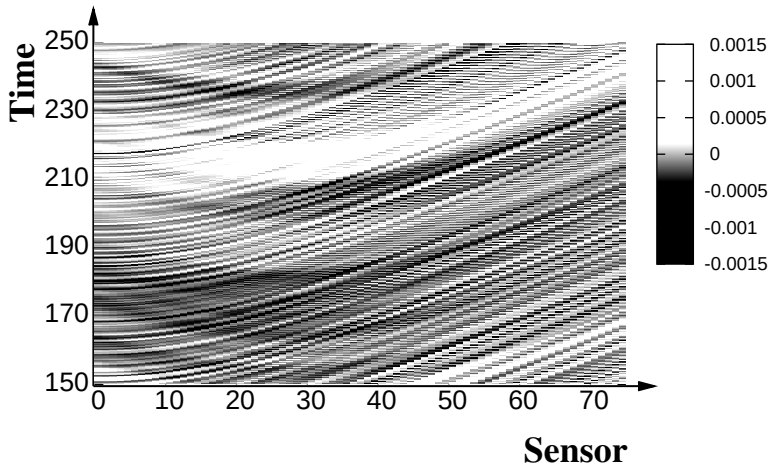

Fig. 3 Visualisation of the aeroacoustic far-field, computed by a Greens functions based Lighthill solver.

3 Coherent structure analysis

3.1 The proper orthogonal decomposition (POD)

A frequently employed method to extract coherent flow structures is represented by POD of the flow velocity $\mathbf{u}$ (see e.g. [26]). In the POD approximation, the velocity fluctuations $\mathbf{u}'$ are approximated by the linear expansion into POD modes $\mathbf{u}_i$

$$\mathbf{u}'(\mathbf{x},t) \approx \sum_{i=1}^{N} a_i^{\mathbf{u}}(t)\,\mathbf{u}_i(\mathbf{x}) \tag{1}$$

where the $a_i := (\mathbf{u}', \mathbf{u}_i)_{\Omega}$ are defined as mode coefficients of the POD modes, latter forming an orthogonal set in the topology of the $\mathbf{L}^2$ Hilbert space with the inner product $(\mathbf{g},\mathbf{f})_{\Omega} := \int_{\Omega} \mathbf{g}\cdot\mathbf{f}\,d\mathbf{x}$.

POD yields least-order modal expansions for any given resolution of total kinetic energy $K_{\Omega}(\mathbf{u}) := \left\langle (\mathbf{u}', \mathbf{u}')_{\Omega} \right\rangle / 2$ where a time-averaging operator $\langle \mathbf{f} \rangle := \lim_{T\to\infty} \frac{1}{2T} \int_{-T}^{T} \mathbf{f}\,dt$ is utilised. The mathematical statement of optimality of POD is that the averaged projection of the hydrodynamic fluctuations onto the POD modes is maximised for a given number of POD modes. The POD modes represent the critical points of the maximum problem

$$\max_{\phi\in\mathbf{H}^{\mathbf{u}},\,(\phi,\phi)_{\Omega}=1} \left\langle \left| \left(\mathbf{u}', \phi\right)_{\Omega} \right|^2 \right\rangle, \tag{2}$$

formulated in a subspace $\mathbf{H}^{\mathbf{u}}$ of the Hilbert space $\mathbf{L}^2$, satisfying regularity, incompressibility and boundary conditions. By calculus of variation, POD modes thus can be defined to be the eigenfunctions of the POD Fredholm integral equation

$$\int_{\Omega} \left\langle \mathbf{u}'(\mathbf{x},t) \otimes \mathbf{u}'(\mathbf{x}',t) \right\rangle \cdot \mathbf{u}_i(\mathbf{x}') \, \mathrm{d}\mathbf{x}' \; = \; \lambda_i^{\mathbf{u}} \, \mathbf{u}_i(\mathbf{x}), \tag{3}$$

where $\otimes$ denotes the outer product of two vectors. Hilbert-Schmidt theory assures, that there is a countable infinity of eigenvalues $\lambda_i^{\mathbf{u}}$, representing the double of total kinetic energy $K_{\Omega}(\mathbf{u})$, resolved by each mode. Typically, POD modes are sorted by the size of these POD eigenvalues, starting from the largest eigenvalue $\lambda_1^{\mathbf{u}}$.

Commonly, the POD decomposition is computed by Sirovich's POD snapshot method [68] based on a given ensemble of velocity snapshots. Application to further fields (e.g. vorticity, aeroacoustic pressure) obtains POD modes which decompose these field most efficiently for the resolution their fluctuation level (in the mentioned examples, these are the time averages of enstrophy and noise respectively). Further details of POD can be found e.g. in [26].

3.2 POD results

Every third time step of the three-dimensional velocity snapshots is employed for POD analysis (1000 snapshots with $\Delta t = 0.3$). First and higher POD modes of the incompressible flow are visualised in the figures 4 and 5. The most energetic structures are dominated by longitudinal streaks downstream from the breakdown of the potential core. Helical structures become more dominant in higher modes. 90% of total kinetic energy of the incompressible jet is resolved by 284 modes (cmp. figure 6). Thus, POD reveals a large number of dynamically important degrees of freedom, which enables flow modelling but is not practical to derive the desired mechanistic understanding (cmp. figure 6). These results are consistent with well-known previous investigations (cmp. e.g. [21, 17]).

A similar POD analysis is employed for the last 1000 snapshots of the vorticity fields ($\Delta t = 0.1$). Here, POD reveals even higher dimensions than the POD analysis of the corresponding velocity snapshot ensemble (1000 snapshots, $\Delta t = 0.1$). 215 POD modes are needed to resolve 90% of time averaged enstrophy while 90% of total kinetic energy of the corresponding velocity is resolved by only 101 POD modes (cmp. figure 7).

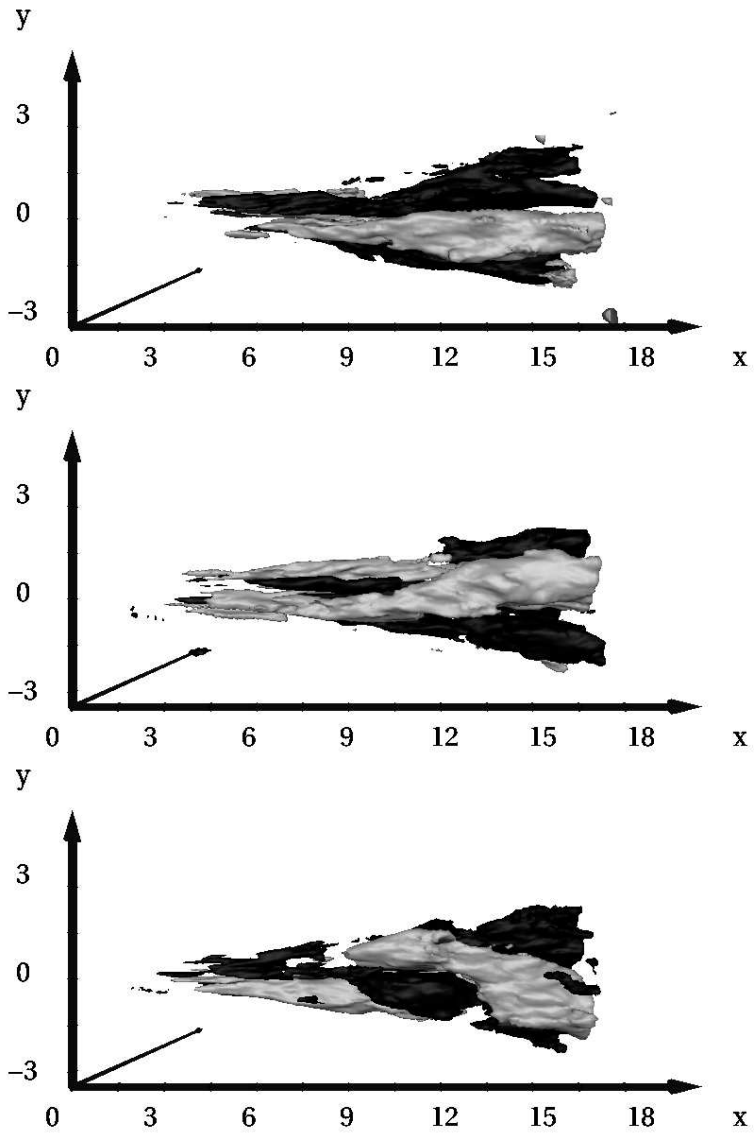

Fig. 4 Visualisation of coherent flow structures. Isosurfaces of the streamwise component of the first three POD modes (1 to 3 from top to bottom) are displayed for positive (light) and negative (dark) values. The grid unit is given by the jet diameter.

4 Wavelet based coherent vortex extraction

4.1 Coherent Vortex Extraction (CVE) method

Coherent vortices are observed in many turbulent flows which seem furthermore to be imbedded in a random background sea. Hence, a denoising procedure may allow

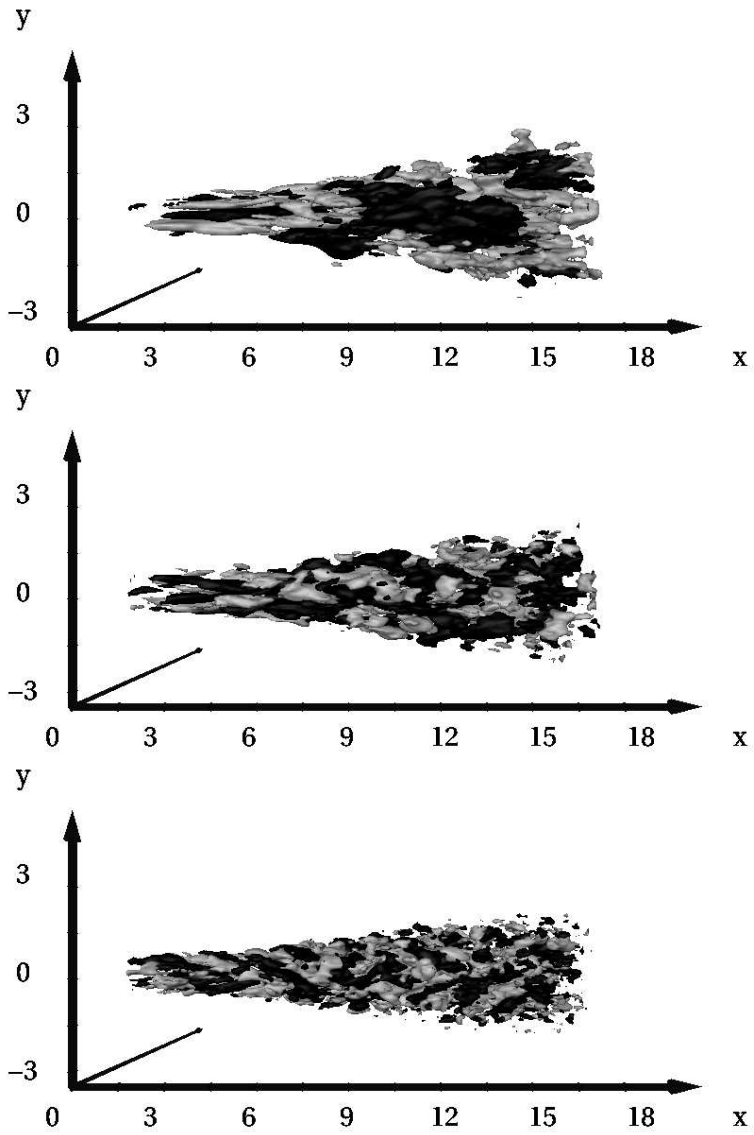

Fig. 5 Visualisation of coherent flow structures. Isosurfaces of the streamwise component of higher POD modes (mode 20, 50 and 100 from top to bottom) are displayed for positive (light) and negative (dark) values. The grid unit is given by the jet diameter.

to eliminate the noise in a given flow realization and the remaining part can then be called coherent vortices. In [15, 14], a wavelet-based method to extract coherent vortices out of both two- and three-dimensional turbulent flows was proposed,

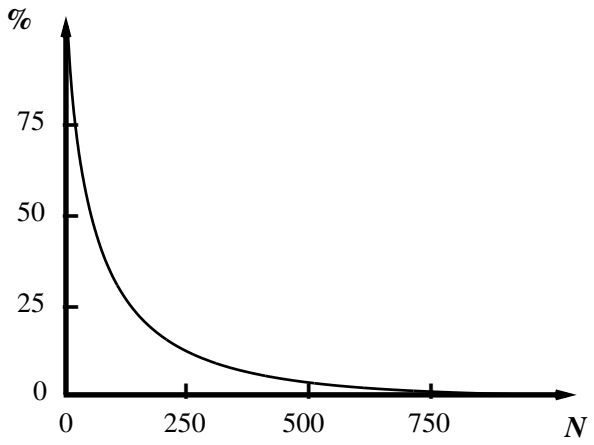

Fig. 6 Residual of total kinetic energy of the POD approximation based on a velocity ensemble of 1000 snapshots over 300 convective time units. Displayed are the percentages of the non-resolved energy over the number of utilised POD modes.

which is directly motivated by denoising. The idea is to apply the orthogonal wavelet decomposition to the vorticity field ω at a given time instant t with resolution N.

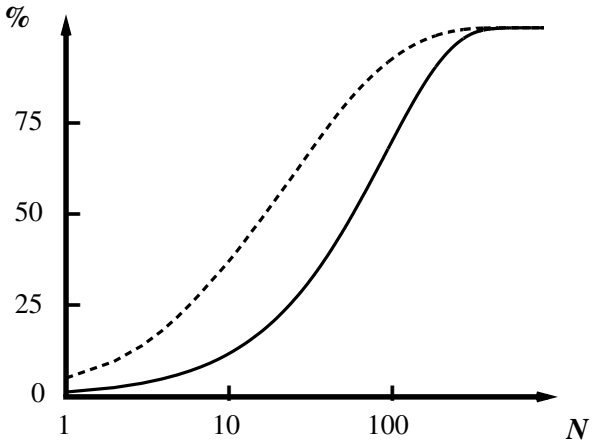

Fig. 7 Resolution of POD of a vorticity field ensemble of 1000 snapshots in a time interval of 100 convective time units. Displayed are the percentages of the resolved average of enstrophy over the number of utilised POD modes (solid line) the latter being scaled logarithmically. This resolution can be compared to the POD resolution of total kinetic energy of the corresponding velocity field (dashed line).

In the following we first fix the notation for the wavelet decomposition of a three dimensional vector field and summarise the main ideas of wavelet based coherent vortex extraction. For more details on the orthogonal wavelet transform, its extension to higher dimensions, we refer the reader to textbooks, e.g., [8]. For more details on the coherent vortex extraction method we refer to the original papers.

A vector field $\mathbf{u}(\mathbf{x})$ is decomposed it into an orthogonal wavelet series

$$\mathbf{u}(x) = \sum_{\lambda \in \Lambda} \widetilde{\mathbf{u}}_\lambda \, \psi_\lambda(\mathbf{x}) \tag{4}$$

where $\mathbf{x} \in \Omega = [0,\ 17.87D] \times [-3.5D,\ 3.5D] \times [-3.5D,\ 3.5D]$, D is the diameter of the jet, and the multi–index $\lambda = (j, i_x, i_y, i_z, d)$ denotes the scale j, the position $\mathbf{i} = (i_x, i_y, i_z)$ and the seven possible directions $d = 1, ..., 7$ of the wavelets. The set $\Lambda = \left\{ \lambda = (j, i_x, i_y, i_z, d), j = 0, ..., i_x, i_y, i_z = 0, ..., 2^j - 1 \text{ and } d = 1, ..., 7 \right\}$ defines the corresponding index set. Due to orthogonality the coefficients are given by $\widetilde{\mathbf{u}}_\lambda = (\mathbf{u}, \psi_\lambda)_\Omega$. The coefficients measure the fluctuations of $\mathbf{u}$ around scale 2^{-j} and around position $\mathbf{i}/2^j$ in one of the seven possible directions. The fast wavelet transform [8] yields a efficient algorithm to compute the N wavelet coefficients $\widetilde{\mathbf{u}}_\lambda$ from the N grid points values of $\mathbf{u}$ and has linear complexity. Here we have chosen the Coiflet 12 wavelet, which has 4 vanishing moments and is appropriate to represent the current flow simulations.

The idea of of the coherent vortex extraction method can be summarised in the following three step procedure:

- *Decomposition:* compute the wavelet coefficients of vorticity $\widetilde{\omega}_\lambda$ using the fast wavelet transform.
- *Thresholding:* apply the thresholding function ρ_ε to the wavelet coefficients $\widetilde{\omega}_\lambda$, thus reducing the relative importance of the coefficients with small absolute value.
- *Reconstruction:* reconstruct the coherent vorticity ω_C from the thresholded wavelet coefficients using the fast inverse wavelet transform. The incoherent vorticity ω_I is obtained by simple subtraction, $\omega_I = \omega - \omega_C$.

The thresholding function ρ corresponds to

$$\rho_\varepsilon(a) = \begin{cases} a \text{ if } |a| > \varepsilon \\ 0 \text{ if } |a| \leq \varepsilon \end{cases} \tag{5}$$

where ε denotes the threshold.

The thresholding parameter ε depends on the variance of the incoherent vorticity σ_n and on the sample size N. The threshold

$$\varepsilon_D = \sigma_n \sqrt{2 \ln N} \tag{6}$$

is motivated from denoising theory [9]. However, the variance of the incoherent vorticity is unknown, and has to be estimated from the available total vorticity ω. As a first guess we take the variance of the total vorticity, which overestimates the vari-

Table 1 Statistical properties of the total, coherent and incoherent vorticity fields of one snapshot at time t=130.1

	N [%]	Z	Z [%]	$\|\|\omega\|\|_{L^\infty}$
Total	100	0.2972	100	11.998
Coherent	4.75	0.2715	91.35	12.304
Incoherent	95.25	0.0257	8.65	2.116

ance of the incoherent vorticity. Thus we split the field into coherent and incoherent parts and then take the variance of the incoherent vorticity as a new improved estimator. In [1] we have developed an iterative algorithm for this task, based on the method presented in [15]. Here we decided to perform one iteration step only which can be justified by the fast convergence of the iterative procedure and by the fact that the computational effort is minimised.

Using the above algorithm, the flow is decomposed into two parts: a coherent flow, corresponding to the coherent vortices, and an incoherent flow, corresponding to the background noise [15]. This decomposition yields $\omega = \omega_C + \omega_I$. Due to orthogonality we have $\langle \omega_C, \omega_I \rangle = 0$ and hence it follows that enstrophy is conserved, *i.e.*, $Z = Z_C + Z_I$ where $Z = \frac{1}{2}\langle \omega, \omega \rangle$.

Let us mention that the complexity of the Fast Wavelet Transform (FWT) is of $O(N)$, where N denotes the total number of grid points.

4.2 CVE results

The CVE method is applied to the vorticity of the turbulent incompressible jet at nondimensional time $t = 130.1$. The resolution of the computation is $N = 128^3$.

The CVE method decomposes the total vorticity ω into coherent vorticity ω_C and incoherent vorticity ω_I. The results of the decomposition are summarised in table 1. Figure 8 shows the enstrophy kept in the N strongest wavelet modes. The threshold is $\varepsilon_D = 1.155$, and the percentage of modes used to represent the coherent component of the vorticity field, a measure for the compression rate, is 4.75%.

Therefore, only a hundred thousand modes instead of two million modes are used to represent the coherent part of the flow field, which resolves more than 91% of the total enstrophy. To gain further insight we now consider the percentage of retained wavelet coefficients at different scale indices j. The scale index j is related to a mean wavenumber $k_j = k_0 2^j$, where k_0 is the centroid wavenumber of the chosen wavelet [11]. The wavelet representation implies that there are $7 \cdot 2^{3j}$ wavelet coefficients at a given scale j. Table 2 shows the percentage of retained wavelet coefficients at the scale index j. At large scales, *i.e.*, for $j \leq 2$, almost all coefficients are retained and correspond to the coherent part. At smaller scales, where the total number of coefficients dramatically increases, the percentage of retained coefficients decreases strongly, and at the smallest scale only about 3% of the coefficients are retained.

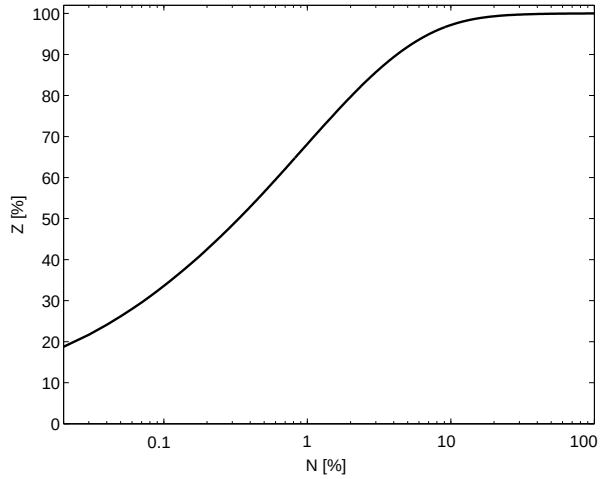

Fig. 8 Resolved enstrophy as a function of the number of retained wavelet coefficient which have been sorted by the order of magnitude. Z and N are normalised with the reference value at full resolution and expressed in percent.

Table 2 Scale-dependent compression rate.

Scale j	$N_{retained}/N_{total}$ [%]	$N_{retained}$	N_{total}
0	100.00	7	7
1	96.43	54	56
2	95.09	426	448
3	60.04	2151	3584
4	28.51	8175	28672
5	12.92	29632	229376
6	3.23	59255	1835008

Figure 9 shows isosurfaces of vorticity at nondimensional time $t = 130.1$. The total vorticity shown in figure 9 (top) is characterised by well developed vortical structures. Those structures are retained in the coherent field, visualised in figure 9 (middle). The incoherent field, shown in figure 9 (bottom), contains no organised vortical structures and resembles noise. Its norm is about a factor 10 smaller with respect to the total vorticity.

The spectral distribution of the total, coherent, and incoherent enstrophy is compared in figure 10. The spectra of the total and coherent fields coincide up to a wave number $k \approx 20$, and a faster decay of the spectrum is observed for the coherent field in the dissipative range with wave-numbers $k > 50$. The spectrum of the incoherent field contains contributions at all wave-numbers but is significant only in the dissipative range. We also observe that the total and coherent spectra exhibit a $k^{1/3}$ range which is in agreement with Kolmogorov's $k^{-5/3}$ law, as the enstrophy spectrum is k^2 times the energy spectrum. The spectrum of incoherent vorticity shows some

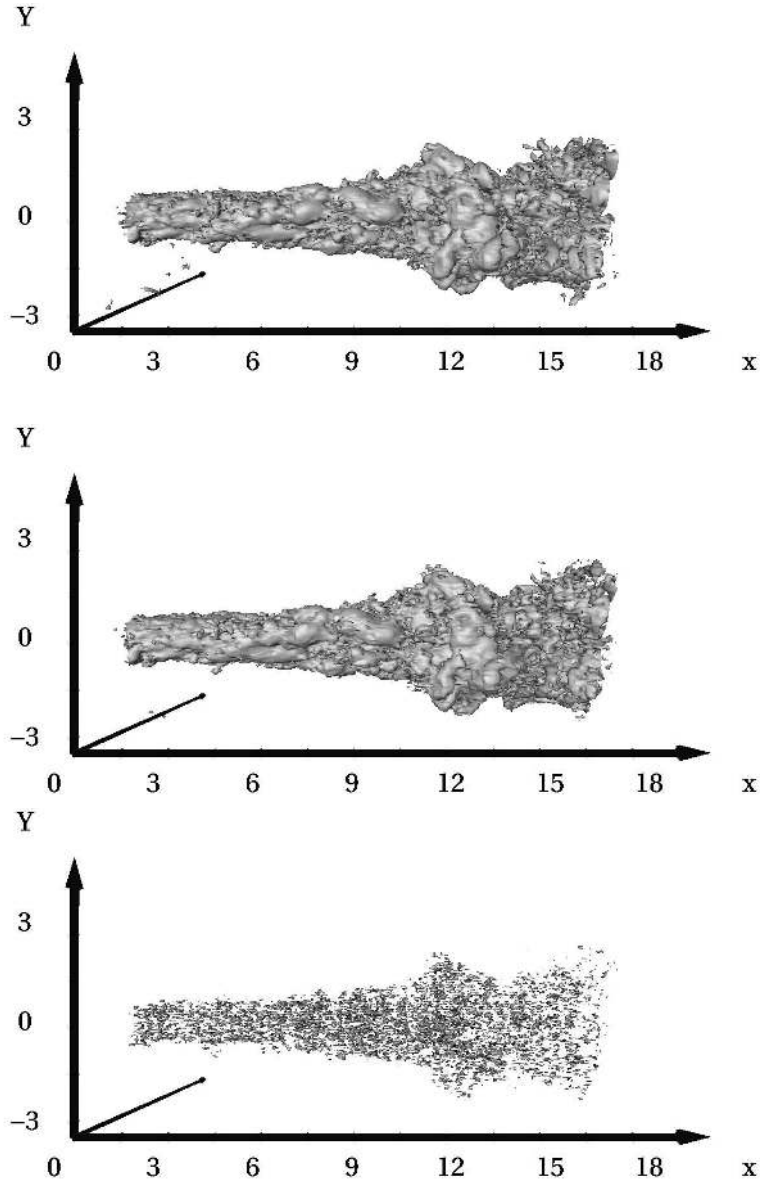

Fig. 9 Isosurfaces of the total (top), coherent (middle) and incoherent (bottom) vorticity. The nondimensional values of the isosurfaces are $|\omega| = 0.7$.

k^4 scaling, which corresponds to energy equipartition, *i.e.* k^2 scaling of the energy spectrum.

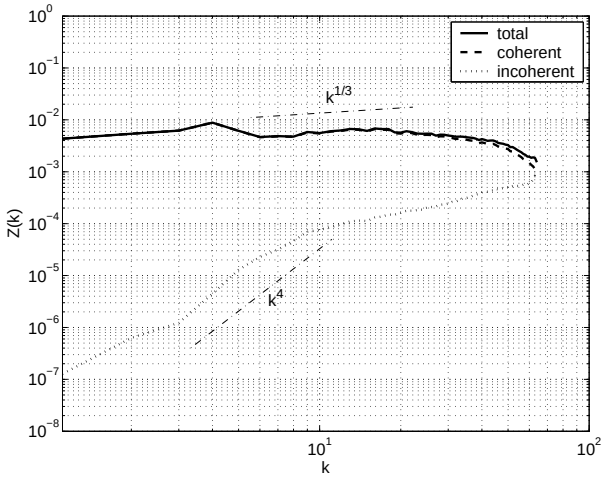

Fig. 10 Enstrophy spectra of total, coherent, and incoherent vorticity. For details, see text.

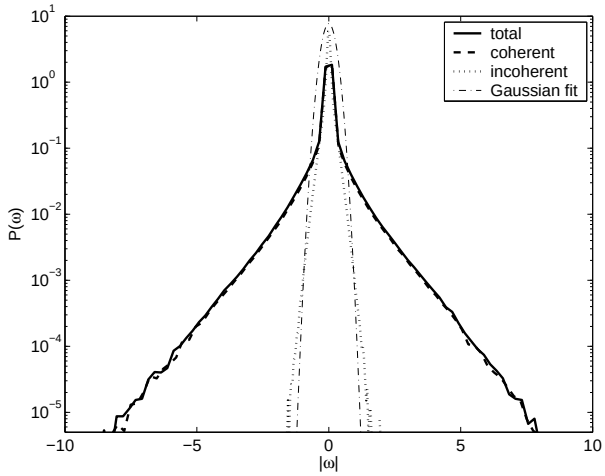

Fig. 11 PDF of total, coherent and incoherent vorticity, together with a Gaussian fit.

A study of the probability density functions (PDF) of vorticity yields information about the higher order statistics of the flow. Figure 11 shows the PDF of total, coherent, and incoherent vorticity. First, we observe that the PDF of the total and coherent vorticity almost perfectly coincide, and exhibit exponential tails. The PDF of the incoherent vorticity has a strongly reduced variance, and agrees reasonably well with the Gaussian.

5 Identification of loud jet flow structures

5.1 The most observable decomposition (MOD)

To obtain the desired physical understanding of jet noise generation, an aeroacoustically optimised extension of POD is proposed, termed most observable decomposition (MOD). This method is described in [61, 60, 29] in detail. Here, a short overview is given. In the following, hydrodynamic fluctuations and the fluctuations of the aeroacoustic far-field are considered to be prefiltered by POD decomposition via the approximations (1) and

$$p'(\mathbf{y},t) \approx \sum_{i=1}^{J} a_i^p(t)\, p_i(\mathbf{y}) \tag{7}$$

in the given domains Ω and Γ of near- and far-field respectively. Modes and mode coefficients of the POD of the aeroacoustic far-field are denoted by p_i and a_i^p, respectively.

The latter POD modes decompose the pressure far-field most efficiently for the resolution the aeroacoustic noise level. The main idea of MOD is to impose this optimality to the the optimality of the MOD approximation

$$\mathbf{u}'(\mathbf{x},t) \approx \sum_{i=1}^{J} a_i^*(t)\, \mathbf{u}_i^*(\mathbf{x}) \tag{8}$$

of the hydrodynamic field, where the sense of optimality is defined by the optimal resolution of the goal functional, given by the correlated level

$$Z_\Gamma^C(\mathbf{u}) := \left\langle \left(p'\left(\mathbf{u}'\right), p'\left(\mathbf{u}'\right)\right)_\Gamma \right\rangle / 2 \tag{9}$$

of fluctuations of the pressure far-field. From this perspective, the question of how to design optimality of MOD requires to know how to model the relationship of hydrodynamic field and pressure far-field.

In the most observable decomposition, a linear relationship between the hydrodynamic and aeroacoustic fluctuations is proposed after the propagation time τ

$$p'(t+\tau) = \mathbf{C}\,\mathbf{u}'(t)\,, \tag{10}$$

where both fluctuation variables can be considered to be represented by the vector of the respective mode coefficients, applying the POD prefilter. Thus, the linear mapping $\mathbf{C}$ from hydrodynamic fluctuations onto fluctuations of the pressure far-field can be identified by linear stochastic estimation utilising the POD coefficients of hydrodynamic field and pressure far-field.

In MOD, it is assumed that the main events of the generation of jet noise are captured in average by the linear mapping defined in equation (10). Validity of this assumption is confirmed by a considerable body of physical evidence: the shear-

Table 3 Minimum principles and control perspectives of the two types of MOD.

MOD variant	'least-residual' MOD (LR-MOD)	'least-energetic' MOD (LE-MOD)
minimum principle of MOD approximation	minimisation of flow attractor residual	minimisation of hydrodynamic fluctuation
control goal	flow reconstruction by a dynamic observer	reduction of total kinetic energy energy causes reduction of correlated noise → energy-based jet noise control design

noise originated from a linear source term of the velocity fluctuations been shown to dominate in free-jets in terms of the hydrodynamic, turbulent pressures [74], and to correlate better with the far-field pressure than the self-noise originated from a quadratic source term of the velocity fluctuations [30, 32, 59, 64, 58, 51]; In [5] it is furthermore demonstrated that the coherent flow structures generate noise via a linear mechanism in the region upstream of the end of the potential core.

The MOD modes are obtained by the pseudoinverse images of the far-field POD modes

$$\mathbf{u}_i^* = \mathbf{C}^- \mathbf{p}_i \,, \tag{11}$$

and employing orthonormalisation. Because the definition of the pseudoinverse is typically not unique, this equation represents an ill-posed problem. Additional constraints are required to modify the problem to become well-posed. Two optimal principles are considered, addressed to flow control purposes as demonstrated in table 3 thus defining two MOD modes variants

Like in the POD approach, analogues of the POD maximum problem (2) and the Fredholm integral equation (3) can be obtained for both MOD variants. The POD eigenvalues of the far-field shall coincide with the MOD eigenvalues, representing the double of the resolved portion of the correlated noise $Z_I^C(\mathbf{u})$ of each mode. Commonly, (LR- or LE-) MOD modes are sorted by the size of the MOD eigenvalues, starting from the largest eigenvalue.

5.2 MOD results

MOD results are obtained based on the POD results of subsection 3.2 and the aeroacoustic far-field data as described in section 2.

Dimension reduction capability by one order of magnitude in comparison to POD dimensions is demonstrated. 90% of correlated noise Z_I^C is resolved by only 33 MOD modes (cmp. Fig. 5.2). This result fits well with an MOD dimension of 24 for the $Ma = 0.9$ jet with the same Reynolds number, obtained in [29]. The first four

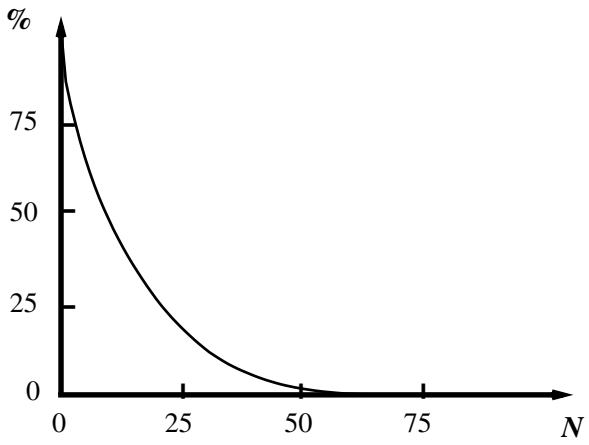

Fig. 12 Residual of correlated noise of the MOD approximation. Displayed are the percentages of the non-resolved correlated noise over the number of utilised (LR- or LE-) MOD modes.

LR-MOD modes are visualised in figure 13, showing dominant helical structures around the breakdown region of the jet potential core reminiscent to results of [16].

6 Galerkin modelling

A low-dimensional Galerkin model of the three-dimensional, incompressible jet is presented in this section. We employ 30 POD modes of the whole domain, representing 39% of total kinetic energy. The Galerkin system

$$\dot{a}_i = \frac{1}{Re} \sum_{j=0}^{30} l_{ij} a_j + \sum_{j,k=0}^{30} q_{ijk} a_j a_k \text{ for } i = 1,\ldots,30,$$

is derived from the POD Galerkin approximation (1) with a standard projection on the Navier-Stokes equations [26]. The system coefficients are defined by $l_{ij} := (\mathbf{u}_i, \Delta \mathbf{u}_j)_{\Omega}$ and $q_{ijk} := (\mathbf{u}_i, \nabla \cdot (\mathbf{u}_j \mathbf{u}_k))_{\Omega}$, using the mean flow $\mathbf{u}_0 := \langle \mathbf{u} \rangle$. To enhance compactness of notation, the coefficient $a_0 \equiv 1$ is introduced as well.

Characteristic frequencies of the POD mode coefficients of the Navier-Stokes attractor are reproduced by the Galerkin model as illustrated in figure 14. Following Rempfer and Fasel [55], neglected fine-scale effects are modelled based on a calibration of modal turbulent eddy viscosities (cmp. [46] for further details). With this model, the coefficients amplitudes coincides as well (cmp. figure 14 again).

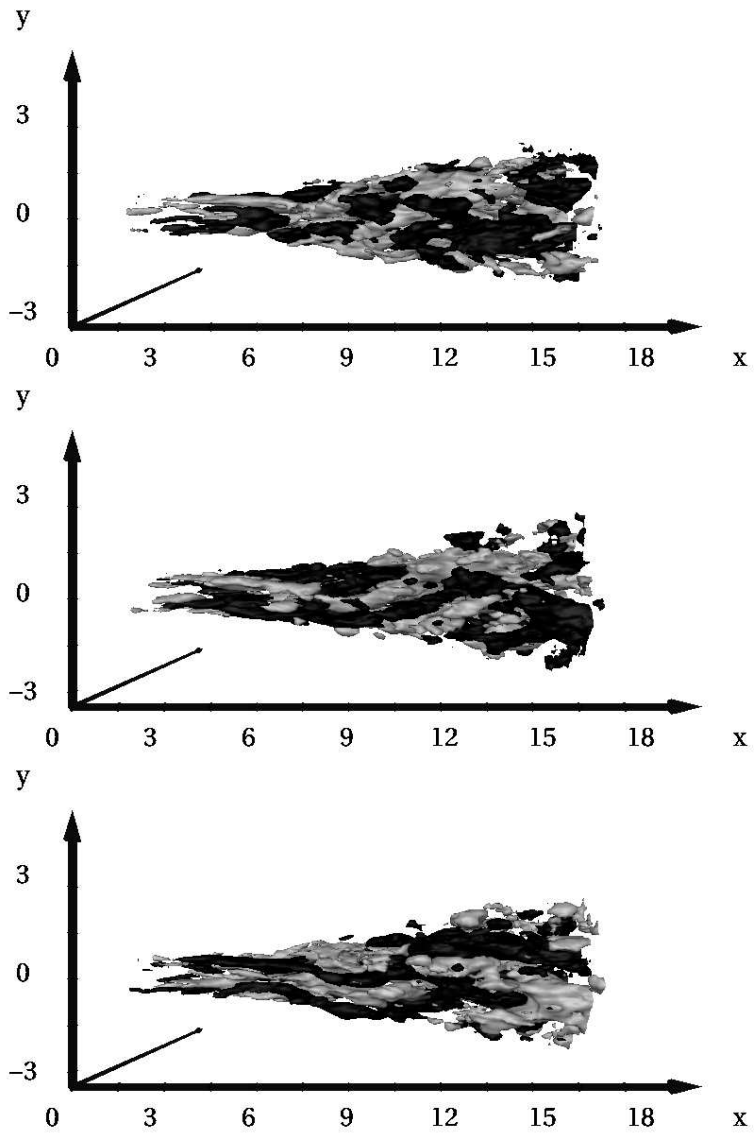

Fig. 13 Visualisation of 'loud' jet flow structures. Isosurfaces of the streamwise components of the first three (from top to bottom) least-residual MOD modes are shown for positive (bright) and negative (dark) values. The grid unit is given by the jet diameter.

7 Outlook to applications of jet noise control

Two key enabler of jet noise control design are represented by the Galerkin system and the LE-MOD approach, enabled by suppression of the total kinetic energy

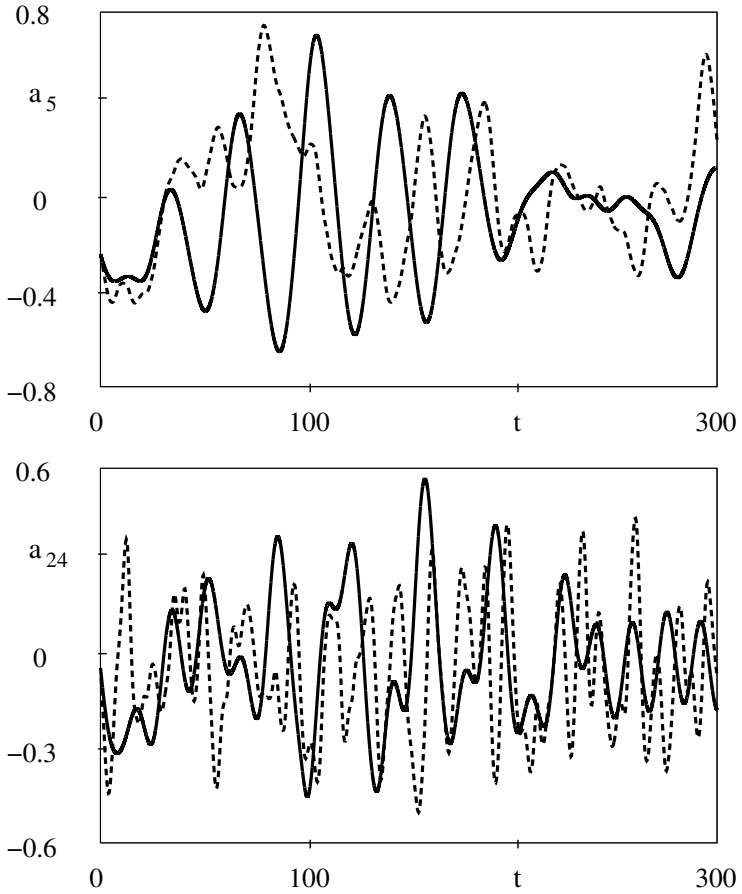

Fig. 14 Two POD Fourier coefficients with low (top) and high (bottom) frequencies over an interval of 300 convective time units. For both coefficients, similar frequency behaviour is observed on the DNS represented Navier-Stokes attractor (dotted line) and in the Galerkin model (solid line).

contained in the 'loud' LE-MOD velocity subspace, which is irreducible in respect to maintain the noise level. Thus energy-based Lyapunov design is pursued for the suppression of the energy flow into the LE-MOD subspace.

As one example of control, we have modelled plasma actuation, which have reduced jet noise in flow control experiments [57] by 0.5 to over 1.0 dB. Two plasma actuators, manipulating respectively the flow in streamwise and transverse direction at the breakdown of the jet potential core, are implemented into a 100 POD mode Galerkin model of the jet flow in thin layer parallel and symmetric to the $z = 0$ plane (cmp. [60]). To identify the Galerkin system, an ansatz of Rempfer [54] is pursued, according to which Galerkin projections can be effected in infinitely thin slices. On this subdomain, 100 POD modes are still required to resolve more than 80% of total

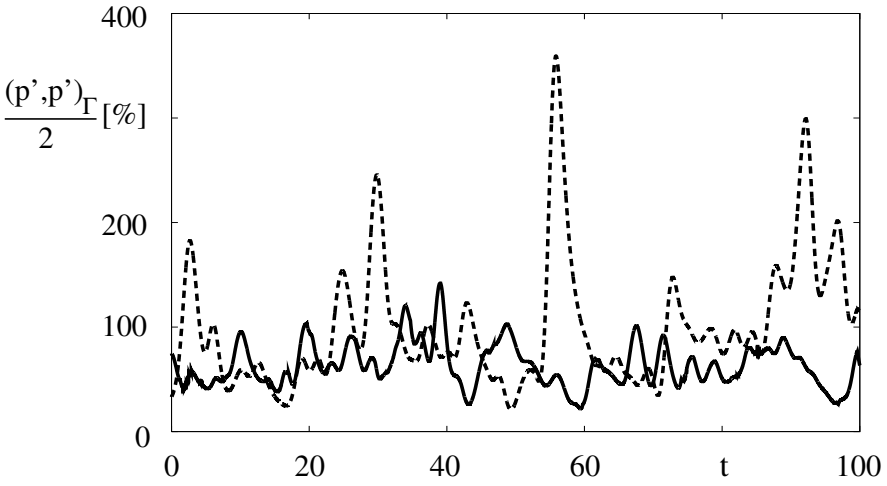

Fig. 15 Noise control via suppression of loud flow structures (LE-MOD modes). Displayed are evolutions of the level of far-field fluctuations (noise) over 100 convective time units. The former are expressed in percent of the correlated noise level Z_Γ^C of the natural jet flow. The most noise generating flow events in the natural Galerkin model dynamics (dashed line) are suppressed by energy-based flow control (solid line). Thus a mean noise reduction by 2 dB is achieved.

kinetic energy. The actuation of the two plasma actuators is implemented employing identification of volume forces as described e.g. in [46]. For stabilisation of the controlled simulation, third order terms are implemented in the Galerkin model.

Noise reduction by approximately 2 dB has been performed. Under action of the plasma actuators, the energy flow into the loud subspace is penalised based on Lyapunov control design. Thus, the most noise generating flow events are mitigated as shown in figure 15.

In future application, a significant enhancement of noise reduction is expected from local actuations at the nozzle exit, implemented in the Galerkin model of the whole three-dimensional jet. Here, moreover, the modelling of the high-dimensional flow residuum via FTT opens the path to the first fully nonlinear infinite horizon control. In future applications. this form of control design is expected to overcome serious challenges of current (locally) linear design with vortex merging and multiple-scale physics.

8 Conclusions

A reduced-order strategy for jet noise control is proposed pursing the path of

(i) identification and dynamic modelling of coherent structures,
(ii) identification of loud structures and

(iii) suppression of loud flow structures.

Coherent structures of the three-dimensional, incompressible jet are identified by POD analysis. 284 POD modes are required to resolve 90% of the total kinetic energy. Nonetheless, the dynamics of the most coherent structures, representing 39% of total kinetic energy, are reproduced by the 30-dimensional Galerkin model.

A wavelet-based coherent vortex extraction method was applied to LES simulations of a free jet. This method allows for an efficient extraction and analysis of vortical structures contained in such flows. It was found that few (4.75%) wavelet coefficients represent the coherent vortices of the flow. The results presented here motivate coherent vortex simulations of turbulent flows for aeroacoustics. First results of CVS for three-dimensional mixing layers are presented in [62] and are promising. Further analysis of vorticity structures, enstrophy spectra and higher-order statistics suggests that the dynamical information of the total field is retained by the coherent field. It can be anticipated that a temporal integration of the coherent field will result in an evolution similar to that of the total flow field. For the incoherent flow field a viscous decay of the fluctuations can be anticipated.

A mechanistic understanding for jet noise control has been extracted using an extension of POD, we term most observable decomposition [29, 61]. The most sound-producing dynamics of turbulent jets are identified by this method. An reduction of dynamically relevant degrees of freedom against POD is achieved from MOD application to the incompressible jet. Two variants of MOD are tailored for the purposes of noise control design.

In a first example of jet noise control, control capability of the proposed ROM strategy is demonstrated achieving an reduction of jet noise by 2 dB. From more comprehensive future investigations including the implementation of experimentally realisable actuations and FTT modelling (see [45]), a significant enhancement of noise reduction is expected.

It should be noted, that the presented methods are applicable to experimental data, e.g. PIV measurements, as well.

Acknowledgements We appreciate valuable stimulating discussions with Boye Ahlborn, Jean-Paul Bonnet, Jacques Borée, Laurent Brizzi, Laurent Cordier, Joël Delville, Andreas Dillmann, Helmut Eckelmann, Dandy Eschricht, Jonathan Freund, William K. George, Elmar Gröschel, Hans-Christian Hege, Peter Jordan, Rudibert King, Oliver Lehmann, Claus-Dieter Munz, Mark Pastoor, Ulrich Rist, Bernd Rummler, Wolfgang Schröder, Jörn Sesterhenn, Oksana Stalnov, Frank Thiele, Charles Tinney, Maja Wänström, Mingjun Wei, and Tino Weinkauf. This work was supported by the Deutsche Forschungsgemeinschaft (DFG) under grants NO 258/1-1, NO 258/2-3 and SCHL 586/1-1. Parts of the CPU time was allocated free by the CNRS supercomputing centre IDRIS under project CP2-80912. Marie Farge, Dmitry Kolomenskiy and Kai Schneider thankfully acknowledge financial support from CNRS, department ST2I and the Agence Nationale de la Recherche project 'M2TFP'. Additionally, Dmitry Kolomenskiy and Kai Schneider are thankful to the Deutsch-Französische Hochschule in Saarbrücken, project 'S-GRK-ED-04-05'. The work of Gilead Tadmor was partially supported by the National Science Foundation (NSF) under grant number 0524070. Moreover all authors acknowledge excellent working conditions and support of the DFG-CNRS Research Group FOR 508 "Noise Generation in Turbulent Flows" and the DFG funded Collaborative Research Center Sfb 557 "Control of Complex Turbulent Shear Flow" at the Berlin Institute of Technology. The 3D flow visualisation has been performed with Amira Software

(Zuse Institute Berlin). We are grateful for outstanding computer and software support from Martin Franke and Lars Oergel.

References

1. A. Azzalini, M. Farge and K. Schneider. Nonlinear wavelet thresholding: A recursive method to determine the optimal denoising threshold. *Appl. Comput. Harm. Anal.*, 18(2):177–185, 2004.
2. M. Bergmann, L. Cordier and J.-P. Brancher. Optimal rotary control of the cylinder wake using proper orthogonal decomposition reduced order model. *Phys. Fluids*, 17:1–21, 2005.
3. C. Bogey, C. Bailly and D. Juvé. Noise investigation of a high subsonic, moderate Reynolds number jet using a compressible large eddy simulation. *Theoret. Comput. Fluid Dyn.*, 16:273–297, 2002.
4. J. Borée. Extended proper orthogonal decomposition: a tool to analyse correlated events in turbulent flows. *Exp. Fluids*, 35:188–192, 2003.
5. F. Coiffet, P. Jordan, J. Delville, Y. Gervais and F. Ricaud. Coherent structures in subsonic jets : a quasi-irrotational source mechanism? *Int. J. Aeroacoustics* 5(1), 67–89, 2006.
6. A. Cohen. *Wavelet methods in numerical analysis*, volume 7 of *Handbook of Numerical Analysis*. P.G. Ciarlet and J.L. Lions (eds.) Elsevier, Amsterdam, 2000.
7. P. Comte, Y. Dubief, C. Bruni, M. Meinke, C. Schultz and T. Rister. Simulation of spatially developing plane and round jets. In E.H. Hirschel (ed.), *Numerical Flow Simulation I, CNRS-DFG Collaborative Research Programme, Results 1996-1998, Notes on Numerical Fluid Mechanics 66*, Vieweg, 301–319, 1998.
8. I. Daubechies. *Ten Lectures on wavelets*. SIAM, Philadelphia, 1992.
9. D. Donoho and I. Johnstone. Ideal spatial adaptation via wavelet shrinkage. *Biometrika*, 81:425–455, 1994.
10. R. Ewert and W. Schröder. On the simulation of trailing edge noise with a hybrid LES/APE method. *J. Sound Vibration*, 270:509–524, 2004.
11. M. Farge. Wavelet transforms and their applications to turbulence. *Ann. Rev. Fluid Mech.*, 24:395, 1992.
12. M. Farge, G. Pellegrino, K. Schneider, A. Wray and B. Rogallo. Coherent vortex extraction in three-dimensional homogeneous turbulence: Comparison between CVS–wavelet and POD–Fourier decompositions. *Phys. Fluids*, 15(10):2886–2896, 2003.
13. M. Farge and K. Schneider. Coherent Vortex Simulation (CVS), a semi–deterministic turbulence model using wavelets. *Flow, Turbulence and Combustion*, 66(4):393–426, 2001.
14. M. Farge, G. Pellegrino and K. Schneider. Coherent vortex extraction in 3D turbulent flows using orthogonal wavelets. *Phys. Rev. Lett.*, 87(5):45011–45014, 2001.
15. M. Farge, K. Schneider and N. Kevlahan. Non–Gaussianity and Coherent Vortex Simulation for two–dimensional turbulence using an adaptive orthonormal wavelet basis. *Phys. Fluids*, 11(8):2187–2201, 1999.
16. J. Freund and T. Colonius. POD analysis of sound generation by a turbulent jet. Submitted to *Int. J. Aeroacoustics.*, 2008.
17. J. Freund and T. Colonius. POD analysis of sound generation by a turbulent jet. *AIAA-paper*, 2002-0072, 2002.
18. J. Freund. Noise sources in a low Reynolds number turbulent jet at Mach 0.9. *J. Fluid Mech.*, 438:277–305, 2001.
19. J. Gerhard, M. Pastoor, R. King, B.R. Noack, A. Dillmann, M. Morzyński and G. Tadmor. Model-based control of vortex shedding using low-dimensional Galerkin models. *AIAA-Paper*, 2003-4262, 2003.
20. S.V. Gordeyev and F.O. Thomas. Coherent structures in the turbulent planar jet. Part 1. Extraction of proper orthogonal decomposition eigenmodes and their self-similarity. *J. Fluid Mech.*, 414:145–194, 2000.

21. E. Gröschel, W. Schröder, M. Schlegel, J. Scouten, B.R. Noack and P. Comte. Reduced-order analysis of turbulent jet flow and its noise source. ESAIM: Proceedings, 16:33–50. Special Issue E. Cancés and J.-F. Gerbeau (eds.) CEMRACS 2005 — *Computational Aeroacoustics and Computational Fluid Dynamics in Turbulent Flows.* Marseille, France, July 18–August 26, 2005, 2007.
22. N. Heinz. Niederdimensionale Modellierung und Kontrolle eines Freistrahls (translated: Low-dimensional modelling and control of a jet). *Diploma thesis, Berlin Institute of Technology, Berlin, Germany*, 2007.
23. L. Henning, M. Pastoor, R. King, B.R. Noack and G. Tadmor. Feedback control applied to bluff body wake. In R. King (ed.): *Active Flow Control. Notes on Numerical Fluid Mechanics and Multidisciplinary Design* 95, Springer, 2007.
24. J.I. Hileman, B.S. Thurow, E.J. Caraballo and M. Samimy. Large-scale structure evolution and sound emission in high-speed jets: real-time visualization with simultaneous acoustic measurements. *J. Fluid Mech.*, 544:277–307, 2005.
25. C. Hoarau, J. Borée, J. Laumonier and Y. Gervais. Analysis of the wall pressure trace downstream of a separated region using extended proper orthogonal decomposition. *Phys. Fluids*, 18(055107), 2006.
26. P. Holmes, J.L. Lumley and G. Berkooz. *Turbulence, Coherent Structures, Dynamical Systems and Symmetry.* First paperback edition. Cambridge University Press, 1998.
27. M.S. Howe. *Theory of Vortex Sound.* Cambridge University Press, 2003.
28. F. Jacobitz, L. Liechtenstein, K. Schneider and M. Farge. On the structure and dynamics of sheared and rotating turbulence: Direct numerical simulation and wavelet based coherent vortex extraction. *Phys. Fluids*, 20(4):045103, 2008.
29. P. Jordan, M. Schlegel, O. Stalnov, B.R. Noack and C.E. Tinney. Identifying noisy and quiet modes in a jet. *AIAA-Paper*, 2007–3602, 2007.
30. D. Juvé, M. Sunyach and G. Comte-Bellot. Intermittency of the noise emission in subsonic cold jets. *J. Sound Vibr.*, 71(3):319–332, 1980.
31. R. King, M. Seibold, O. Lehmann, B.R. Noack, M. Morzyńksi and G. Tadmor. Nonlinear flow control based on a low dimensional model of fluid flow. In T. Meurer et al. (eds.): *Control and Observer Design for Nonlinear Finite and Infinite Dimensional Systems. Lecture Notes in Control and Information Sciences*, 322:369–386, 2005.
32. H.K. Lee and H.S. Ribner. Direct Correlation of Noise and Flow of a Jet. *J. Acoust. Soc. Am.*, 52(5):1280–1290, 1972.
33. M. Lesieur, O. Métais and P. Comte. *Large-Eddy Simulations of Turbulence.* Cambridge University Press, 2005.
34. F. Li, A. Banaszuk, G. Tadmor, B.R. Noack and P.G. Mehta. A reduced order Galerkin model for the reacting bluff body flame holder. *AIAA-Paper*, 2006-3487, 2006.
35. M.J. Lighthill. On sound generated aerodynamically: I. General theory. *Proc. R. Soc. Lond. A*, 211:564–587, 1952.
36. J. Little, M. Debiasi, E. Caraballo and M. Samimy. Effects of open-loop and closed-loop control on subsonic cavity flows. *Phys. Fluids*, 19(065104), 2007.
37. S. Maurel, J. Borée and J.L. Lumley. Extended Proper Orthogonal Decomposition: Application to Jet/Vortex Interaction. *Flow, Turbulence and Combustion*, 67:125–136, 2001.
38. M. Meinke, W. Schröder, E. Krause and T.R. Rister. A Comparison of Second- and Sixth-Order Methods for Large-Eddy Simulations. *Computer and Fluids*, 21:695–718, 2002.
39. C. Meneveau. Analysis of turbulence in the orthonormal wavelet representation. *J. Fluid Mech.*, 232: 469–520, 1991.
40. D. Moreno, A. Korthapalli, M.B. Alkislar and L.M. Lourenco. Low-dimensional model of a supersonic rectangular jet. *Phys. Rev. E*, 69(026304):1–12, 2004.
41. M. Morzyński, W. Stankiewicz, B.R. Noack, R. King, F. Thiele and G. Tadmor. Continuous mode interpolation for control-oriented models of fluid flow. In R. King (ed.), *Active Flow Control*, Papers contributed to the Conference "Active Flow Control 2006", Berlin, Germany, September 27–29, 2006. Springer-Verlag, *Notes on Numerical Fluid Mechanics and Multidisciplinary Design* 95: 260–278, 2007.

42. M. Morzyński, W. Stankiewicz, B.R. Noack, F. Thiele and G. Tadmor. Generalized mean-field model for flow control using a continuous mode interpolation. *AIAA-Paper*, 2006-3488, 2006.
43. S. Narayanan, P. Barooah and J.M. Cohen. Dynamics and control of an isolated jet in cross flow. *AIAA J.*, 41:2316–2330, 2003.
44. S. Narayanan, B.R. Noack and E. Meiburg. Reduced-order dynamical modeling of sound generation from a jet. *AIAA-Paper*, 2002–0073, 2002.
45. B.R. Noack, M. Schlegel, B. Ahlborn, G. Mutschke, M. Morzyński, P. Comte and G. Tadmor. A finite-time thermodynamics of unsteady fluid flows. *J. Non-Equilib. Thermodyn.*, 33(2):103–148, 2008.
46. B.R. Noack. Niederdimensionale Galerkin-Modelle für laminare und transitionelle freie Scherströmungen (transl: Low-dimensional Galerkin models of laminar and transitional free shear flows). *Habilitation thesis, Fakultät V – Verkehrs- und Maschinensysteme, Berlin Institute of Technology, Germany*, 2005.
47. B.R. Noack, P. Papas and P.A. Monkewitz. The need for a pressure-term representation in empirical Galerkin models of incompressible shear flows. *J. Fluid Mech.*, 523:339–365, 2005.
48. B.R. Noack, I. Mezić, G. Tadmor and A. Banaszuk. Optimal mixing in recirculation zones. *Phys. Fluids*, 16(4):867–888, 2004.
49. B.R. Noack, K. Afanasiev, M. Morzyński, G. Tadmor and F. Thiele. A hierarchy of low-dimensional models for the transient and post-transient cylinder wake. *J. Fluid Mech.*, 497:335–363, 2003.
50. N. Okamoto, K. Yoshimatsu, K. Schneider, M. Farge and Y. Kaneda. Coherent vortices in high resolution direct numerical simulation of homogeneous isotropic turbulence : A wavelet viewpoint. *Phys. Fluids*, 19(115109):1–13, 2007.
51. J. Panda, R.G. Seasholtz and K.A. Elam. Investigation of noise sources in high-speed jets via correlation measurements. *J. Fluid Mech.*, 537:349–385, 2005.
52. M. Pastoor, L. Henning, B.R. Noack, R. King and G.Tadmor. Feedback shear layer control for bluff body drag reduction. *J. Fluid Mech.*, 608:161–196, 2008.
53. C. Picard and J. Delville. Pressure velocity coupling in a subsonic round jet. *Int. J. Heat Fluid Flow*, 21:359–364, 2000.
54. D. Rempfer. Empirische Eigenfunktionen und Galerkin-Projektionen zur Beschreibung des laminar-turbulenten Grenzschichtumschlags (transl.: Empirical eigenfunctions and Galerkin projection for the description of the laminar-turbulent boundary-layer transition). *Habilitation Thesis, Universität Stuttgart*, 1995.
55. D. Rempfer and F.H. Fasel. Dynamics of three-dimensional coherent structures in a flat-plate boundary-layer. *J. Fluid Mech.*, 275:257–283, 1994.
56. H.S. Ribner. Quadrupole correlations governing the pattern of jet noise. *J. Fluid Mech.*, 38:1–24, 1969.
57. M. Samimy, J.-H. Kim, J. Kastner, I. Adamovich and Y. Utkin. Active Control of a Ma=0.9 Jet for Noise Mitigation Using Plasma Actuators. *AIAA J.* 45:890–901, 2007.
58. M. Schaffar and J.P. Hancy. Investigation of the noise emitting zones of a cold jet via causality correlations. *J. Sound Vibr.* 81(3):377–391, 1982.
59. T.D. Scharton and P.H. White. Simple Pressure Source Model of Jet Noise. *J. Acoust. Soc. Am.* 52(1):399–412, 1972.
60. M. Schlegel, B.R. Noack, P. Jordan and G. Tadmor. Least-order modal flow decompositions for aerodynamic and aeroacoustic goal functionals. *Proceedings of the 2nd Int. Conf. on Jets, Wakes and Separated Flows, Berlin Institute of Technology, Berlin, Germany*, 2008.
61. M. Schlegel, B.R. Noack, O. Lehmann, E. Gröschel, W. Schröder, M. Wei, J. Freund and P. Jordan. Least-order flow representations, optimised for aeroacoustics and aerodynamics. Manuscript in preparation for publication in *J. Fluid Mech.*, 2008.
62. K. Schneider, M. Farge, G. Pellegrino and M. Rogers. Coherent vortex simulation of three-dimensional turbulent mixing layers using orthogonal wavelets. *J. Fluid Mech.*, 534:39–66, 2005.
63. J.M. Seiner. A new rational approach to jet noise reduction. *Theoret. Comput. Fluid Dyn.*, 10:373–383, 1998.

64. J.M. Seiner and G. Reetoff. On the distribution of source coherency in subsonic jets. *AIAA-paper* 1974-4:1–14, 1974.
65. S.G. Siegel, J. Seidel, C. Fagley, D.M. Luchtenburg, K. Cohen and T. McLaughlin. Low-dimensional modelling of a transient cylinder wake using double proper orthogonal decomposition. *J. Fluid Mech.*, 610:1–43, 2008.
66. S.G. Siegel, S. Aradag, J. Seidel, K. Cohen and T. McLaughlin. Low Dimensional POD Based Estimation of a 3D Turbulent Separated Flow. *AIAA-Paper*, 2007-0112, 2007.
67. S. Siegel, K. Cohen and T. McLaughlin. Feedback control of a circular cylinder wake in experiment and simulation. *AIAA-Paper*, 2003-3571, 2003.
68. L. Sirovich. Turbulence and the dynamics of coherent structures, Part I: Coherent structures. *Quart. Appl. Math.*, XLV:561–571, 1987.
69. M. Soteriou. Vortex element method — expansion about incompressible flow computation of noise generation by subsonic shear flows — the impact of external forcing. *J. Turb.*, 4:1–9, 2003.
70. M. Soteriou, R. Reba and T. Maeder. Numerical study of the impact of streamwise vorticity on noise generation by jet flows. *AIAA-Paper*, 2002-2480, 2002.
71. G. Tadmor, B.R. Noack and M. Morzyński. Control oriented models and feedback design in fluid flow systems: A review. Invited paper, *Proceedings of the 14th Mediteranean Conference on Control and Automation*, 2006.
72. G. Tadmor, B.R. Noack, M. Morzyński and S. Siegel. Low-dimensional models for feedback flow control. Part II: Observer and controller design. *AIAA-Paper*, 2004-2409, 2004.
73. C.E. Tinney, M.N. Glauser and L.S. Ukeiley. Low-dimensional characteristics of a transsonic jet. Part 1. Proper orthogonal decomposition. *J. Fluid Mech.*, 612:101–141, 2008.
74. C.E. Tinney, P. Jordan, J. Delville, A.M. Hall and M.N. Glauser. A time-resolved estimate of the turbulence and sound source mechanism in a subsonic jet flow. *J. Turbulence* 8(1), 1–20, 2007.
75. P. Yan, M. Debiasi, X. Yuan, E. Caraballo, A. Serrani, H. Özbay, J.M. Myatt and M. Samimy. Modeling and Feedback Control for Subsonic Cavity Flows: A Collaborative Approach. In *Proc. of the 44th IEEE Conference on Decision and Control and European Control Conference CDC-ECC'05,* 5492–5497, 2005.

Index